This article has been accepted for publication in IEEE Transactions on Medical Robotics and Bionics. This is the author's version which has not been fully edited and content may change prior to final publication. Citation information: DOI 10.1109/TMRB.2025.3646763

Reconfigurable Soft Exoskeleton for Shoulder Support Using Tendon-Driven Underactuation

Francesco Missiroli[1*], Alessandro Ciaramella[2], Luca Radaelli[3], Emanuele Rambaldi[4], Antonio Frisoli[5], Maura Casadio[4], and Lorenzo Masia[1]

***Abstract*—This study presents a soft, wearable shoulder exosuit designed to assist shoulder abduction and flexion through adaptive gravity compensation. In contrast to traditional rigid exoskeletons that often restrict natural movement and are limited to controlled environments, the proposed system features a lightweight, tendon-driven architecture that preserves mobility while providing effective support during shoulder-intensive activities. The exosuit integrates a dual-motor Bowden cable actuation system with a real-time control strategy that dynamically aligns assistive forces with the user's voluntary motion. This responsive design reduces muscular effort and supports sustained activity by adapting assistance levels in real time. Experimental evaluations with eight healthy participants demonstrated significant reductions in muscle activation, namely 36% in the anterior deltoid, 29% in the medial deltoid, and 27% in the trapezius. Prioritizing portability, modularity, and user comfort, the exosuit offers a compelling alternative to bulkier assistive systems. By combining a soft, wearable form factor with synchronized, multi-degree-of-freedom assistance, it highlights a promising direction for shoulder-assistive technologies suited for daily and occupational use.**

***Index Terms*—Human-machine interfaces; Wearable Robots; Control for Soft Robots.**

I. Introduction

The human shoulder is a highly mobile and versatile joint, essential for performing a wide range of daily and occupational upper-limb tasks such as reaching, lifting, and object manipulation. This mobility stems from the complex interplay between the glenohumeral joint and scapulothoracic articulation. Together, these structures enable exceptional freedom of movement[1], [2]. However, this anatomical complexity poses significant challenges for mechanical assistance: wearable devices must provide effective support while preserving natural mobility and preventing joint misalignment or discomfort [3], [4].

Developing effective wearable assistive technologies for the shoulder remains an open challenge in several engineering scenarios, including accommodating multiple degrees of freedom (DoFs), managing inter-subject variability in shoulder kinematics, and balancing actuation performance, weight, and wearability[5], [6]. Despite advances, existing systems often lack the ability to provide effective assistance across multiple degrees of freedom without compromising wearability or natural mobility. This leaves a gap for devices that balance lightweight design, adaptable control, and comprehensive shoulder support. While traditional rigid exoskeletons address shoulder support through powerful actuators and constrained kinematic chains, they often do so at the expense of user comfort, adaptability, and range of motion, rendering them limited for real-world use[7], [5].

Passive shoulder-support systems, such as spring-based occupational exoskeletons, have shown effectiveness in reducing muscular fatigue during repetitive overhead work [8], [9]. Yet,

Fig. 1. *FALCO*. The device was designed to assist with shoulder flexion and adduction. The exosuit consisted of a wearable orthosis and a lumbar support protector, housing motors, a battery pack, and electronics. A force sensor (5) and two IMU sensors (4) were used to measure the interaction force and arm kinematics, respectively. The actuation unit (3) housed a Bluetooth low-energy module that connected the sensors with the embedded controller responsible for driving the two motors actuating the device.

[1]Francesco Missiroli and Lorenzo Masia with the Munich Institute for Robotics and Machine Intelligence (MIRMI), Technical University of Munich (TUM), 80992, Munich, Germany.

[2]Alessandro Ciaramella is with the Department of Information Engineering, University of Pisa, Largo L. Lazzarino 1, 56122 Pisa, Italy.

[3]Luca Radaelli is with the Department of Mechanical Engineering, Politecnico di Milano, 23900 Lecco, Italy.

[4]Emanuele Rambaldi and Maura Casadio are with the Department of Computer Science, Bioengineering, Robotics and Systems Engineering (DIBRIS), University of Genova, 16145, Genoa, Italy.

[5]Antonoio Frisoli is with the Institute of Mechanical Intelligence, Sant'Anna School of Advanced Studies, 56127, Pisa, Italy.

* corresponding author: francesco.missiroli@tum.de

they lack the dynamic adaptability necessary for varied or complex shoulder movements and cannot finely tune assistance to user-specific biomechanics, limiting their effectiveness in variable tasks such as lifting, reaching, or combined joint movements.[10]. Recent quantitative studies demonstrate that powered or semi-passive mechanisms can outperform passive counterparts by reducing muscle activation and delaying fatigue through real-time, task-specific assistance [11], [12].

In recent years, soft, compliant exosuits have emerged as promising alternatives. These devices use lightweight textile materials combined with tendon- or pneumatic-driven actuation to assist movement while enhancing wearer comfort and mobility [13], [14]. The compliant design of soft exosuits minimises motion constraints and improves wearability, making them well-suited for prolonged use in occupational and daily living contexts[15], [16]. However, the inherent compliance introduces challenges such as nonlinear force transmission, friction losses in Bowden cable systems, and variable human-device coupling, which complicate precise force control and real-time responsiveness [17], [18]. Overcoming these limitations remains a core challenge in soft robotic exosuits, particularly for systems that aim to provide precise, responsive, and multi-DoF support using cable-driven mechanisms [19], [20].

Among the leading soft shoulder exosuits, Harvard's pneumatic textile actuator-based system assists shoulder abduction and flexion, achieving up to 40% reductions in muscle activation during targeted tasks and demonstrating the potential of soft actuation for muscle fatigue mitigation [21]. ETH Zurich's tendon-driven exosuit employs a motorised Bowden cable system focused primarily on a single degree of freedom and highlights the feasibility of tendon-driven actuation, though challenges remain in achieving multiple DoF assistance and precise dynamic force control [22]. Both systems illustrate key advancements but also underline ongoing limitations in control, adaptability and full shoulder mobility support.

To address these challenges, we present the Fully Actuated Lightweight Controlled Orthosis (F.A.L.C.O.) 1, a novel soft shoulder exosuit designed to provide adaptive gravity compensation during shoulder abduction and flexion. F.A.L.C.O. integrates a dual-motor tendon-driven actuation mechanism within a textile-based wearable structure, enabling reconfigurable geometry that dynamically aligns assistive forces with the user's voluntary movements. Leveraging real-time kinematic feedback, the system's advanced control algorithm synchronizes assistance with user intent, balancing the advantages of tendon-driven actuation, lightweight, flexible force transmission, with an innovative mechanical layout to maintain natural range of motion without sacrificing support effectiveness. To our knowledge, FALCO represents one of the first systems to implement dual-motor reconfigurability within a tendon-driven soft architecture, enabling simultaneous alignment of force vectors and multi-DoF shoulder support in real time.

Unlike previous soft exosuits that typically employ single-motor actuation or fixed tendon routing, FALCO introduces a dual-motor coordinated actuation mechanism combined with a cantilever-based reconfigurable transmission. In this setup, one motor generates assistive tension while the second dynamically adjusts the tendon's geometry to maintain alignment with the user's shoulder motion. This coordinated strategy allows the system to continuously reorient the assistive force in real time, providing effective gravity compensation across multiple planes of movement.

Additionally, the addition of a passively decoupled cantilever joint and a circular sliding module represents a key mechanical innovation preserving natural shoulder mobility. This combination of mechanisms makes FALCO capable of maintaining lightweight wearability while delivering adaptive, multi-DoF assistance.

To validate the system, we conducted experimental trials with healthy subjects performing tasks that involved the shoulder motion in dynamic and semi-static conditions. Electromyography (EMG) data from key shoulder muscles and endurance assessments confirmed F.A.L.C.O.'s capacity to reduce muscular effort and delay fatigue, highlighting its potential for a broad range of occupational and daily living applications.

While our experimental validation was conducted in controlled laboratory settings, the F.A.L.C.O. exosuit's lightweight, adaptive assistance holds promising potential for reducing muscular fatigue and enhancing endurance during daily living activities and occupational tasks involving prolonged or repetitive shoulder use.

This study aims to validate FALCO's effectiveness in reducing muscular effort and delaying fatigue during shoulder-intensive tasks in healthy users. In doing so, we address critical gaps in the current state of the art, particularly the lack of adaptable, ergonomic exosuits capable of synchronizing with natural human motion across multiple planes. Our findings contribute to advancing wearable robotics by demonstrating an integrated design approach combining mechanical innovation, sensing, and adaptive control for multi-DoF shoulder assistance. The findings provide valuable insights into advancing lightweight, user-synchronised, and ergonomically wearable assistive technologies.

II. Hardware Design

The project aimed to create a system capable of accurately monitoring and supporting shoulder kinematics, particularly within the 0 to 90° range of elevation commonly to counteract the gravitational effort of the joint during daily activities. To achieve this main target, we developed a self-aligning device. The design prioritizes providing mechanical advantages across a wide range of motions while maintaining a compact form. Additionally, a tendon-driven approach was chosen for its ability to generate substantial forces and torques while remaining lightweight and compact.

The overall design of the FALCO comprises eleven 3D-printed components, with one component, the *cantilever*, standing out (Fig. 2). This cantilever is specifically conceived to house two cylindrical joints insisting on the same axis of rotation, allowing the wire to pass through seamlessly without impeding the passive rotation of the mechanism. Its primary function is to passively reconfigure the proximal anchor point and provide enough leverage to transmit the electromechanical power of the motor to the user via Bowden cable transmission.

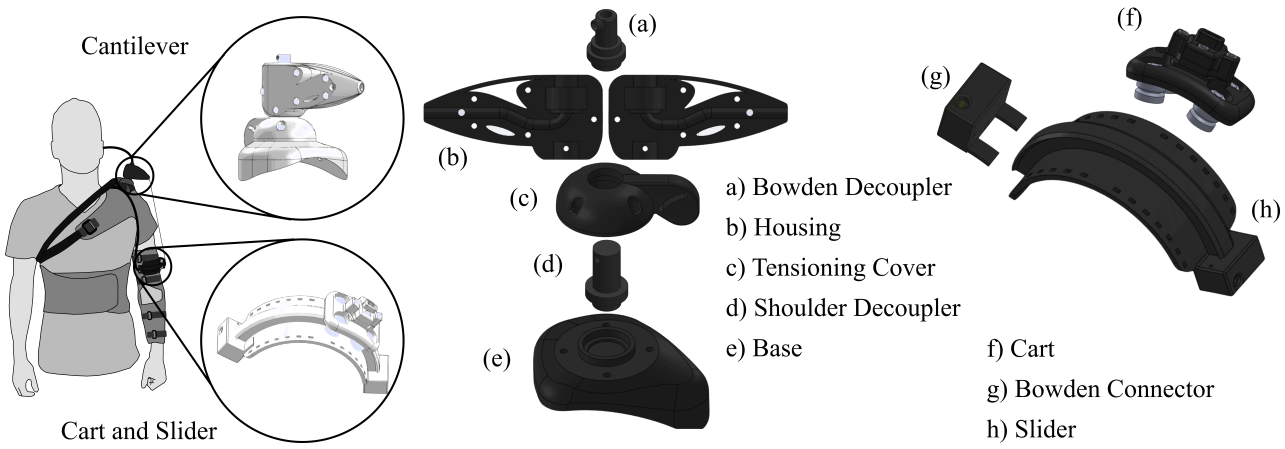

Fig. 2. *Design* and main components of the shoulder exosuit. The compact, lightweight structure includes a cantilever (a-e) with dual cylindrical joints (a and d) to allow seamless Bowden cable transmission, enhancing mechanical efficiency while preserving natural shoulder motion. On the right side, the cart (f) and slider (h) mechanism, in charge of orientation adjustments, ensuring dynamic adaptation to user movements for intuitive, gravity-compensated support.

Additionally, four bearings are strategically positioned to allow free rotation of the element and effectively isolate the forces transmitted by the Bowden cable. This configuration was specifically conceived to minimize nonlinearities and friction losses in the Bowden transmission by decoupling the cable path from transverse loading and ensuring smooth cable routing through passive rotational joints. These mechanical decoupling strategies mitigate the hysteresis typically observed in tendon-driven systems, improving force fidelity at the user interface. While this configuration may seem to introduce unnecessary degrees of freedom, it was essential to ensure efficient cable passage within the device and achieve the desired decoupling.

The two cylindrical joints of the cantilever serve respectively as a Bowden Decoupler, to separate the transverse forces exerted by the Bowden tube on the structure, and as a Shoulder Decoupler, sharing the same rotation axis as the previous joint to enable passive movement of the mechanism in the transverse plane of the cantilever.

The second component of the mechanism is a cart and slider located at the lower part of the user's brachium. It has two primary functions: reconfiguring the anchor point to place it optimally to counteract gravitational forces on the user's arm, and transmitting the suit force to the user.

The slider's design was based on previous arm circumference measurements for the brace to ensure an optimal fit. Consequently, the slider had a "dovetail" shape, covering approximately 100° of the arm's circumference. The ends of the slider were designed thoughtfully to allow easy mounting of the cart.

The cart itself was crafted to match the slider's curvature and featured a dedicated space for attaching the anchor point. This anchor point comprised two parts: the first part was directly fixed to the cart and included a semicircular channel to house the cable, while the second part was placed on top, securing the cable with two additional screws.

Four bearings with dovetail profiles (negative in this case) were attached to the cart to achieve a smooth and controlled motion of the mechanism. These bearings facilitated longitudinal movement along the slider and effectively prevented any transverse slippage.

Concerning the delineation of shoulder movements, the decision to rely on two motors to assist in the desired range of motion involves their division of tasks as follows:

- One motor used to provide pulling assistive force;
- The second one geometrically configures the mechanism to align the tendon on the plane of motion.

Drawing inspiration from shoulder biomechanics, the initial motor aids the user in counteracting the gravitational force exerted on the user's arm, akin to the muscles involved in arm flexion and abduction movements, specifically the Anterior and Medial Deltoid muscles.

Moreover, to support the underactuated system, a second motor is employed to adjust the direction of the assisting force based on the user's intended motion.

The second motor operates by reconfiguring the position of the cart situated on the slider using a tendon-driven mechanism. Two cables are attached to the cart, with their ends directed onto a motor pulley in opposing directions of rotation. As a result, the rotational motion of the motor is converted into linear movement of the cart along the slider.

In detail, the mechanism aiding the shoulder movement comprises two flat brushless motors (T-Motor, AK60-6, 24 volts, 6:1 planetary gear-head reduction, Cube Mars actuator, Nanchang, Jiangxi, China). One motor drives a single-layer pulley (diameter $35\,\mathrm{mm}$) around which the artificial tendon is wound (Black Braided Kevlar Fiber, KT5703-06, capable of withstanding a maximum load of $2.2\,\mathrm{kN}$, Loma Linda, CA, USA), while the second motor enables the movement of the cart using a double-layer pulley with cables routed in both clockwise and anticlockwise directions.

Shoulder assistance from the actuation stage to the exosuit is facilitated through a Bowden cable (Shimano SLR, with a diameter of $5\,\mathrm{mm}$, Sakai, Ōsaka, Japan), connecting the motor pulleys to the anchor points positioned on the cantilever and the cart. Additionally, the artificial tendon is equipped with a force sensor (ZNLBM-1, maximum load capacity $50\,\mathrm{kg}$, Bengbu Zhongnuo Sensor, China) linked to the cart, which

measures the interaction between the exosuit and the user's arm. The control architecture and power supply are enclosed within a 3D-printed structure.

To detect the user's motion, the sensing network of the shoulder exosuit comprehends two IMUs (IMU, Bosch, BNO055, Gerlingen, Germany), and two microcontrollers (Feather nRF52 Bluefruit, from Adafruit Industries, New York City, USA) providing Bluetooth low energy communication between the sensors and the actuation control unit positioned on the device's back, as extensively detailed in [23].

Each IMU sensor transmits arm posture quaternions via the Feather board, while the load cell detects cable tension. Data is transmitted to the other Feather board wired to the control stage through a proprietary Bluetooth Low Energy serial protocol (BLE UART, Nordic Semiconductors, Trondheim, Norway).

The receiver unpacks the buffered data from the sensing units on the user's arms and communicates them via I2C with an Arduino MKR 1010 WiFi (Arduino, Ivrea, Italy), responsible for the real-time control unit operation. Operating at a frequency of 100 hertz, the Arduino board manages the real-time controller implemented in a MATLAB/Simulink application (MathWorks, Natick, Massachusetts, USA). Furthermore, it dispatches motor commands via CAN-bus to the actuation stage.

III. Real-time controller

Beginning with the FALCO's mechanical design and functionality, the primary focus was synthesizing a model-based gravity compensation controller. The development process started by creating a kinematic model of the user's arm, followed by dividing the control loop into two separate units that work in parallel and synergistically, reflecting the hardware design. The control algorithm has been developed assuring three main targets:

- Provide adequate assistance in supporting the shoulder motion counteracting the gravitational force.
- Detect the user's intention to provide supporting force according to the 3D orientation of the arm.
- Allow the exosuit to move in symbiosis with the wearer with minimal interference force.

As depicted in Fig4, the control architecture is decoupled into two different control loops to control independently the two actuators present in the device, namely the *Tensioning Control* and the *Translating Control* loops.

A. Kinematic model

The initial aim is to estimate the torques exerted on the shoulder joint due to gravity. Before proceeding, the following assumpption are made: first, the arm is modelled as a kinematic chain composed of rigid bodies connected by joints. Second, the hand is assumed to be rigidly attached to the forearm, ignoring the wrist joint. Finally, the shoulder joint is simplified to a 3 Degrees of Freedom (DoF) spherical joint.

We adopted a fixed XYZ Euler angles parametrization to describe the joint orientation. ϕ_1, ϕ_2 and ϕ_3 are the Euler angles according to the following convention [24]:

$$ {}^{w}_{u}R = \begin{bmatrix} c(\phi_3)c(\phi_2) & c(\phi_3)s(\phi_2)s(\phi_1) - s(\phi_3)c(\phi_1) & c(\phi_3)s(\phi_2)c(\phi_1) + s(\phi_3)s(\phi_1) \\ s(\phi_3)c(\phi_2) & s(\phi_3)s(\phi_2)s(\phi_1) + c(\phi_3)c(\phi_1) & s(\phi_3)s(\phi_2)c(\phi_1) - c(\phi_3)s(\phi_1) \\ -s(\phi_2) & c(\phi_2)s(\phi_1) & c(\phi_2)c(\phi_1) \end{bmatrix} \quad (1) $$

This matrix describes the rotation of the upper-arm solidal frame u to the absolute world frame w.

It has been pointed out in Section II that the proposed exosuit provides 2-DoF assistance to the shoulder, thus we have to determine a mapping between the Euler angles convention and a 2-parameter representation corresponding to the actuated DoFs.

According to the exosuit mechanical design the two coordinates of interest for the shoulder parametrization are the two angles here described in Figure 3:

- α: shoulder elevation angle defined as the angle between the absolute z-axis and the z-axis of the upper arm solid frame.
- β: arm longitude angle defined with the following steps:
  - defining a transversal circumference centered in the origin of the upper arm solid frame;
  - considering the point of the circumference characterised by the greatest component along the absolute z-axis (highest point from the ground);
  - the angle of interest is the one that the segment that locates the point at issue w.r.t. the origin of the solid frame creates with the solid y-axis.

Moreover, to obtain a comprehensive model of the upper-limb biomechanics, we defined as θ the elbow flexion angle corresponding to the angle between the absolute z-axis and the z-axis of the forearm solid frame.

From 1 we can derive the coordinate $\alpha \in [0, \pi]$:

$$ \alpha = acos(c(\phi_2)c(\phi_1)) \quad (2) $$

To calculate the coordinate β we consider the parametrization of a circumference with unitary radius, centered in the origin of the solid frame and project it on the vertical axis of the world frame:

$$ {}^{u}P_u = \begin{bmatrix} s(\eta) & c(\eta) & 0 \end{bmatrix}^{\mathsf{T}} \quad (3) $$

$$ {}^{w}P^{z}_{u} = \begin{bmatrix} 0 & 0 & 1 \end{bmatrix} {}^{w}_{u}R \, {}^{u}P_u = -s(\eta)s(\phi_2) + c(\eta)c(\phi_2)s(\phi_1) \quad (4) $$

By isolating the z-component of the circumference projected on the world frame and performing the partial derivative in η we obtain:

$$ \left. \frac{\partial {}^{w}P^{z}_{u}}{\partial \eta} \right|_{\eta=\beta} = -c(\beta)s(\phi_2) - s(\beta)c(\phi_2)s(\phi_1) = 0 \quad (5) $$

By rearranging the equation, we can isolate the variable of interest:

$$ \tan(\beta) = -\frac{s(\phi_2)}{c(\phi_2)s(\phi_1)} \quad (6) $$

With $\beta \in [-\pi/2, \pi/2]$, this relation can be explicitly expressed:

$$ \beta = atan(-\frac{s(\phi_2)}{c(\phi_2)s(\phi_1)}) \quad (7) $$

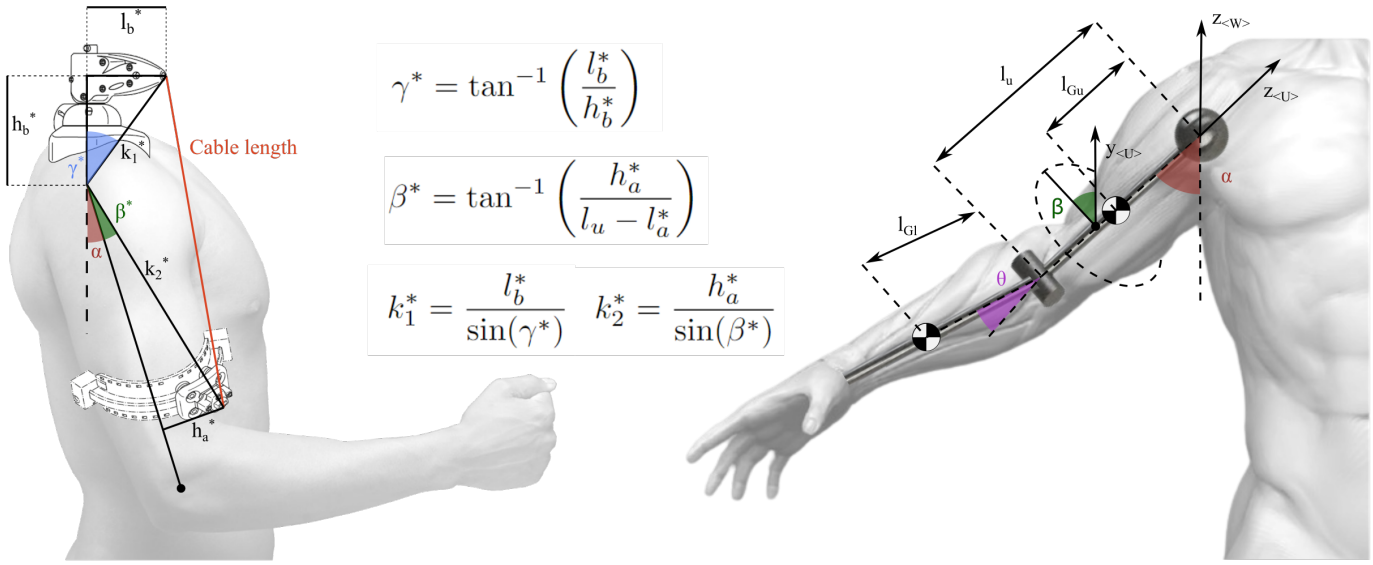

Fig. 3. *Parametrization.* Main parameters and anatomical landmarks used for the parametrization and control of the FALCO shoulder exosuit. The illustration highlights key biomechanical parameters, including center of mass of the arm, position of the anchor points with respect to anatomical landmarks, and angles used in the parametrization, as well as the customized anthropometric measurements integral to the *tensioning* and *translating* control loops. These parameters enable precise alignment and torque assistance tailored to the user's movements, optimizing both fit and functionality.

To add the effect of gravitational force into our model, we need to determine the z-coordinate of the center of mass of each arm segment in the world frame. By inspection (Fig. 3), the z-coordinate of the center of mass of the upper segment of the arm is:

$$z_u = -l_{Gu}c(\phi_2)c(\phi_1); \tag{8}$$

Whereas the z-coordinate of the center of mass of the lower segment resulted in:

$$z_l = -l_{Gl}c(\phi_2)c(\phi_1+\theta) - l_u c(\phi_2)c(\phi_1); \tag{9}$$

where l_{Gu} is the distance of the center of mass of the upper segment of the arm from the origin of the last frame of the XYZ sequence, l_{Gl} is the distance of the center of mass of the lower segment of the arm from the origin of the elbow frame, l_u is the length of the upper segment of the arm.

B. Tensioning Control

The *Tensioning Control* loop comprised a high-level controller to estimate the assistive reference torque (τ_r), needed to provide gravity compensation, and to compare it with the torque measured by the load cell (τ_i). A low-level admittance controller tracks the error between the two torques and uses it as a reference signal for the motor command.

1) High-Level Controller: The high-level controller computes the reference torque τ_r from a biomechanical model of the arm, accounting for the 3D orientation of the joints (i.e. shoulder and elbow). We adopted the classical equation of motion to compute torque at the joints[25]:

$$\tau(q(t)) = M(q(t))\ddot{q}(t) + C(q(t),\dot{q}(t)) + G(q(t)); \tag{10}$$

where q, $\dot{q}$ and $\ddot{q}$ represent the Lagrangian coordinates of our system obtained through the previous parametrization. The inertial and mass properties of the arm are described by the matrix $M(q(t))$, $C(q(t),\dot{q}(t))$ is the vector of Coriolis and centrifugal forces and $G(q(t))$ is the vector of gravitational force scaled on subject anthropometry. These parameters are individualized for each user based on their anthropometric measurements (e.g., arm segment lengths and estimated segment masses), ensuring that the control model and resulting assistive torque are properly scaled to the user's body geometry.[18]

Since the movements of the arm are usually slow and smooth, meaning that the joints' velocities and accelerations are low, 10 can be written in quasi-static conditions as:

$$\tau(q(t)) \approx G(q(t)) = \frac{\partial U}{\partial q}; \tag{11}$$

In particular, the reference torque is expressed as:

$$\tau_r = \frac{\partial U}{\partial \alpha}; \tag{12}$$

The gravity-compensation torque then only depends on the potential energy U of the kinematic chain:

$$\begin{gathered} U = m_u g z_u + m_l g z_l = \\ -gc(\phi_2)\{c(\phi_1)[(m_u l_{Gu} + m_l l_u) + m_l l_{Gl} c(\theta)] - s(\phi_1)[m_l l_{Gl} s(\theta)]\} \end{gathered} \tag{13}$$

To simplify the notation, we will substitute the terms in the formula$(m_u l_{Gu} + m_l l_u)$ with K_{ul} and $m_l l_{Gl}$ with K_l. By substituting the relationships shown in 2,7 into U, the potential energy can be expressed as a function of both the actuated coordinates and the elbow angle:

$$U = -g\{c(\alpha)[K_{ul} + K_l c(\theta)] - s(\alpha)c(\beta)[K_l s(\theta)]\} \tag{14}$$

Starting from this equation and considering that U does not depend on $\dot{\alpha}$, the gravity-compensation torque (presented in 12) can be easily derived:

This article has been accepted for publication in IEEE Transactions on Medical Robotics and Bionics. This is the author's version which has not been fully edited and content may change prior to final publication. Citation information: DOI 10.1109/TMRB.2025.3646763

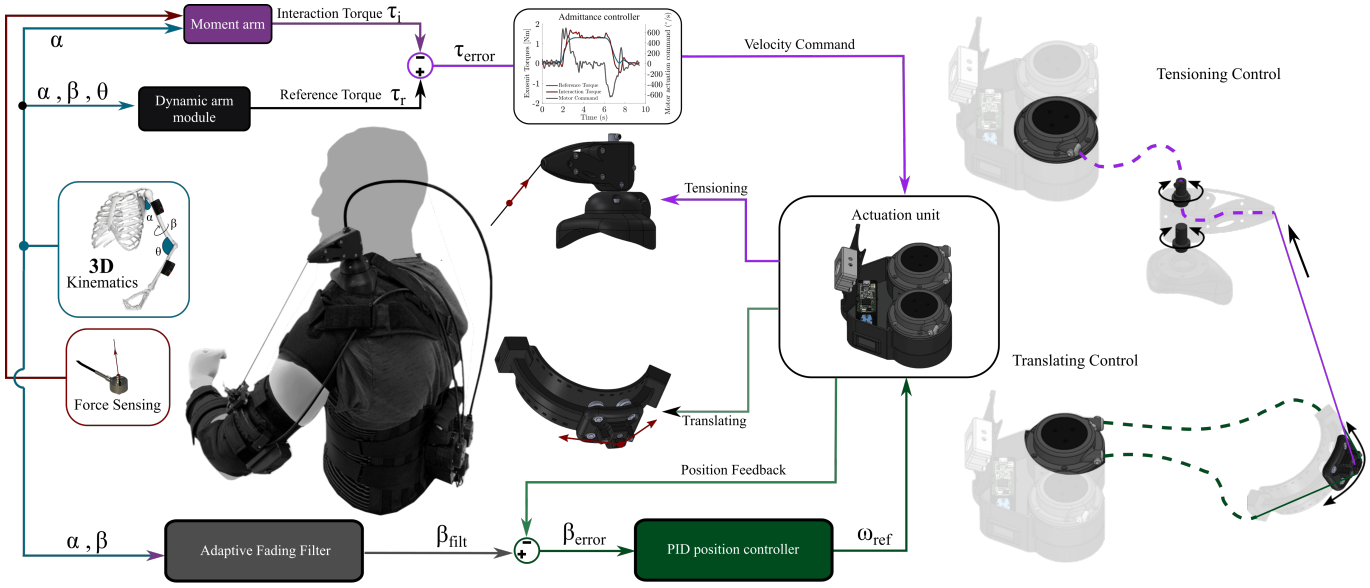

Fig. 4. *Control framework.* The exosuit assists the wearer through a gravity compensation control, reducing the effort required to lift the shoulder against gravity. The *tensioning control* incorporates a biomechanical model tailored to the user's anthropometry. This control estimates a reference torque, which is then compared with the interaction torque measured by a force sensor. The torque tracking error is processed through an admittance controller to generate a motor velocity command, which is sent to the actuation stage to provide the necessary assistance. On the other side, the *translating control* consists of a position control loop that adjusts the position of the distal anchor point on the cart, aligning it with the highest elevation point of the slider.

$$\tau_r = \frac{\partial U}{\partial \alpha} = g\{s(\alpha)[K_{ul} + K_l c(\theta)] + c(\alpha)c(\beta)[K_l s(\theta)]\} \quad (15)$$

It is worth noticing that this formulation does not consider the damping due to the biological articulations.
To overcome this problem, we added two positive damping contributions to the gravity-compensation torque. Specifically, out of the three angles present in equation 15, only α and θ are relevant to model the damping. Therefore, the two additional terms depend on the respective velocities.
The final formulation for the gravity-compensation torque is thus:

$$\tau_r = g\{s(\alpha)[K_{ul} + K_l c(\theta)] + c(\alpha)c(\beta)[K_l s(\theta)]\} + D_1\dot{\alpha} + D_2\dot{\theta} \quad (16)$$

where D_1 and D_2 are empirically determined. As previously pointed out, the *Tensioning Control* is an indirect force control and therefore, given the torque reference, it needs a torque feedback to evaluate the tracking error. To do that, a model of the arm with the exosuit on is derived (Fig. 3). As pointed out by the figure, the model is planar, thus the resulting model is 2-dimensional. Due to the reconfigurable nature of the proposed exosuit, the passive cantilever and the slider anchor point always lay on the same plane, where the elevation angle α is defined. Under this assumption, the shoulder joint is then considered a revolute joint and the arm is considered an assembly of non-deformable bodies connected by joints. Moreover, the exosuit is assumed to be stationary relative to the arm. Last, the cantilever is always perfectly parallel to the ground.

Based on the following simplifications, all the terms marked with an asterisk are fixed. Out of these quantities, the four that are supposedly easier to derive from biomechanical assumptions (l_b^*, h_b^*, l_a^*, h_a^*), are used to derive the other ones.
Hereafter the remaining terms from the arm model are evaluated as a function of l_b^*, h_b^*, l_a^*, h_a^*, by taking advantage of the right triangle trigonometry 3. The next step is to compute the cable length k as a function of the elevation angle. According to the law of cosines:

$$k(\alpha) = \sqrt{k_1^{*2} + k_2^{*2} + 2k_1^* k_2^* cos(\gamma^* + \beta^* + \alpha)} \quad (17)$$

The derivative for the elevation angle of the cable displacement is evaluated to describe how the displacement varies according to the change of the shoulder elevation angle.

$$J(\alpha) = \frac{\partial k}{\partial \alpha} = -\frac{k_1^* k_2^* sin(\gamma^* + \beta^* + \alpha)}{\sqrt{k_1^{*2} + k_2^{*2} + 2k_1^* k_2^* cos(\gamma^* + \beta^* + \alpha)}} \quad (18)$$

Finally, the estimated assistive torque delivered at the virtual joint is given by the equation:

$$\tau_i = J(\alpha) f \quad (19)$$

where f is the cable tension retrieved from the load cell.

2) Low-Level Controller: As mentioned above, mechanical admittance describes the force/velocity relationship at the end-effector of a kinematic chain, making it a particularly effective and well-established control method for upper-limb assistive devices[26].In this application, the admittance controller compensates for user-specific variations in coupling stiffness and residual cable friction by adapting motor velocity commands to the measured interaction torque. This ensures stable assistance and compliant behavior even in the presence of nonlinear transmission effects or individual anatomical variability. In particular, in the Laplace domain, the relation is:

$$\frac{\dot{x}(s)}{\tau(s)} = R(s) = B_a + \frac{D_a}{s} + M_a s \tag{20}$$

where $\tau(s)$ represents the torque reference, and M_a, B_a and D_a are design parameters.
In the developed control, the admittance relation is directly applied. The control then has the same form as a PID control whereby: B_a, D_a and M_a are regarded as proportional, integral and derivative gains, respectively, empirically tuned. The PID controller gains were initially estimated using the Ziegler–Nichols tuning method and subsequently fine-tuned through iterative experimental validation to achieve stable torque tracking and smooth assistive behavior across users.

C. Translating control

As mentioned above, the "translating control" module comprises two main sub-modules: the Exponential adaptive filter and the PID position controller.

1) Adaptive Fading Filter: The adaptive fading filter is used to smooth out the abrupt changes of the β coordinate when the elevation angle is close to 0.
The recursive equation of the filter is a convex combination of the newest input data with the previous output:

$$y[n] = (1 - \lambda)x[n] + \lambda y[n-1] \tag{21}$$

where $y[n]$ is the output at the current time step n, $x[n]$ is the current input and $y[n-1]$ is the output at the previous time step. The fading factor λ, instead, is a variable scalar value between $\lambda_{min} > 0$ and $\lambda_{max} < 1$, which determines the cut-off frequency of the filter that increases according to the value. It is selected based on the elevation angle to make the system less responsive to noise, where β is close to singularity configuration.

A λ value between two extrema λ_{min} and λ_{max} is selected based on the elevation angle: if α is small, the selected value of λ is close to 1, so as to make the system less responsive to abrupt changes in β. On the contrary, if α is big, the selected value of λ is close to 0, determining a high system responsiveness.
The relation between λ and α results from the interpolation with a custom sigmoid function to have a smooth transition:

$$\lambda(\alpha) = (1 - \frac{1}{1 + e^{k(\alpha - \alpha_0)}})\lambda_{max} + \frac{1}{1 + e^{k(\alpha - \alpha_0)}}\lambda_{min} \tag{22}$$

where α_0 is the interpolation midpoint and k regulates the steepness of the curve.

2) PID position controller: Since the cart position on the rail directly depends on the longitude angle, after the filtering, the latter is used as a reference signal for a PID position controller. The filtered β is then compared with the feedback motor position. Once the error between the filtered β and the feedback motor position has been determined, this is fed into the proper PID controller.
Even in this case, the three parameters of the controller are tuned by using the Ziegler-Nicholson tuning rule.

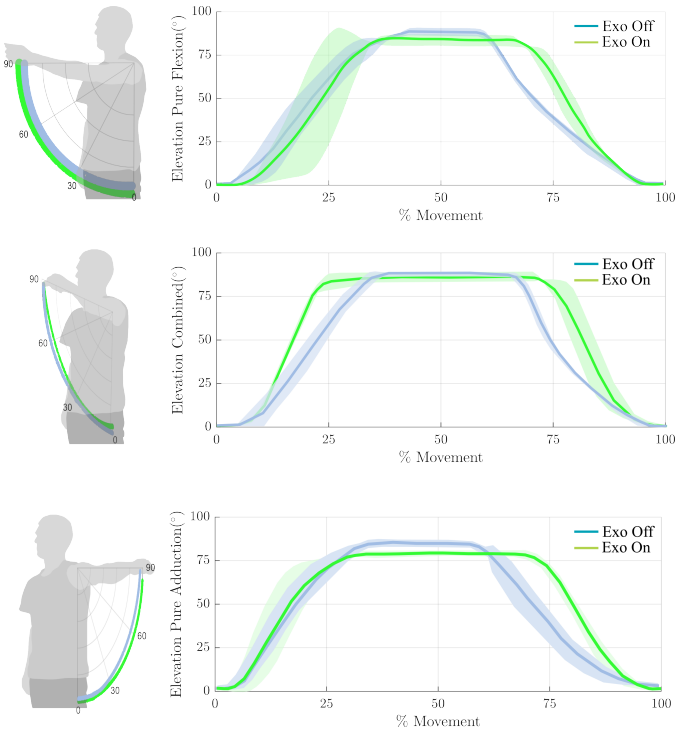

Fig. 5. *ROM* evaluation of the shoulder exosuit. From top to bottom: Evaluation of shoulder flexion/extension angles, illustrating the exosuit's assistance across a full flexion and extension cycle; Mixed motion assessment, capturing the exosuit's response to combined shoulder movements; and Pure abduction/adduction motion, showing the exosuit's capability to accommodate lateral movements with accurate tracking and support.

IV. Experiments

Eight healthy participants were enrolled in the experiment (all males, age 26.88 ± 3.72 years, mean $\pm$ SD, body weight $79.63 \pm 16.18\,\mathrm{kg}$ and height $1.79 \pm 0.10\,\mathrm{m}$). Inclusion criteria were based on no evidence or known history of musculoskeletal or neurological diseases, and exhibiting normal joint range of motion and muscle strength. All experimental procedures were carried out in accordance with the Declaration of Helsinki on research involving human subjects and were approved by the IRB of Heidelberg University (Nr. S-311/2020). All subjects provided explicit written consent to participate in the study. Data acquisition followed the protocol extensively described in a previous related work[23]. We employed a DAQ board (Quanser QPIDe, Markham, Ontario, Canada) to collect kinematics data from the control unit. This data was then employed to provide real-time instructions and motion feedback displayed on a graphical interface (GUI) during testing. Muscle activity was monitored using a multi-channel, wireless surface EMG system (Delsys Trigno, Natick, MA, USA), recording signals from the six selected muscles involved in shoulder motion. The monitored muscles included the *biceps brachii*, *triceps brachii*, *anterior* and *medial* sections of the *deltoid*, *trapezius* and *latissimus dorsi*. Electrode placements followed the SENIAM guidelines.

A. Experimental Protocol

The study consisted in repeated measurements, where participants, wearing the exosuit, performed three functional tasks

This article has been accepted for publication in IEEE Transactions on Medical Robotics and Bionics. This is the author's version which has not been fully edited and content may change prior to final publication. Citation information: DOI 10.1109/TMRB.2025.3646763

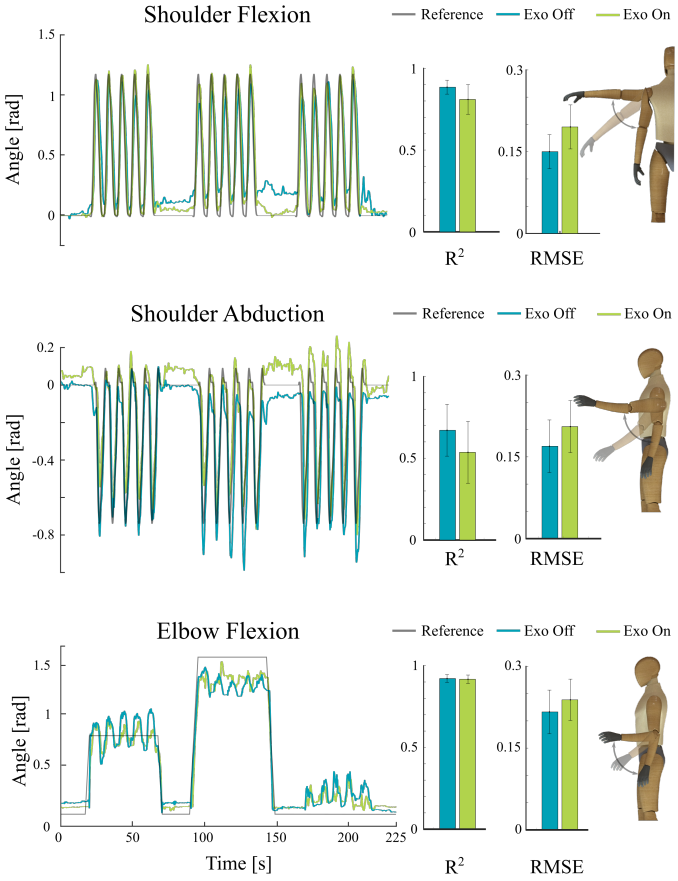

Fig. 6. *Kinematics* evaluation of the shoulder exosuit during the dynamic task. From top to bottom, the plots show shoulder flexion angle, shoulder abduction, and elbow flexion. On the left, temporal plot of a representative subject performing the task, illustrating the tracking accuracy of each joint angle. On the right, cumulative performance metrics across all subjects, displaying the R^2 and RMSE for both Exo Off and Exo On conditions, highlighting the exosuit's impact on movement accuracy and control.

in different conditions with and without exosuit assistance. Each task was performed in all of the two following conditions: "*Exo Off*", where the exosuit was worn but unpowered and "*Exo On*", where the exosuit was powered and controlled using the biomechanical model of the human arm. The experiment was designed to test the device and the controller in terms of Range Of Motion(ROM), muscle activity change, and tracking accuracy. The tasks were named as follows:

1. ROM assessment;
2. Dynamic Task;
3. Static Task.

The order of the conditions was randomized across subjects; to avoid the onset of muscular fatigue, participants rested for $10\,\mathrm{min}$ between the tasks. Before starting, participants performed a $5\,\mathrm{min}$ familiarisation phase with the device to get accustomed to using the device, performing free movements.

1) ROM assessment: The ROM assessment was devised to evaluate the device's capabilities. Human kinematics were estimated from recordings of the positions of 7 reflective markers, placed on the participants by using a stereophotogrammetric system (Qualisys 5+, Qualisys AB, Göteborg, Sweden). Data recorded with the motion capture enabled the calculation of body angles by measuring the distance between each marker. Markers were strategically placed on specific parts of the body, including:

- one marker on the knuckle of the middle finger of the hand;
- two on the wrist (epiphysis ulnaris and radialis);
- two on the elbow (epiphysis ulnaris and radialis);
- one on the acromion;
- one at the C7 level.

Nine movements were performed, three for each axis of study, covering a range of motion between $0°$ and $90°$relevant to counteract gravity in activities of daily living (ADLs). Data collected from these movements were analyzed using an OpenSim inverse-kinematics tool [27]. Inverse kinematics was utilized to determine angles, and the ROM was computed for each movement type, encompassing flexion-extension, abduction-adduction, and combined actions.

2) Dynamic Task: The dynamic task is designed to evaluate both the tracking capability and muscular activation during arm movements, with and without the assistance of the exosuit. To assess the suit effect on the shoulder complex motions while keeping a controlled environment, we selected a movement involving variable α and β angles. This movement entails performing a circular motion with the arm while keeping it within the space defined by the body's frontal and sagittal planes. To control participants' movements throughout the task, they were instructed to carry out repetitive motions, imitating the motion of a virtual avatar displayed in a 3D GUI on a screen placed in front of the subject. The GUI presented a live depiction of the participant's limbs, overlaid on the avatar's limbs, with the avatar adjusted to a transparency of 30%. The dynamic test comprises three sets of three trials. The sets are characterised by three different elbow-angle values: $0°$, $45°$ and $90°$. Each trial consists of performing five circular movements as previously described, by keeping the elbow at the angle that characterizes the trial. The arm should move approximately at $0.52 rad/s$, representing the typical shoulder angular velocity in ADLs [28]. A $20s$ rest separates the trials. The three sets of trials, each characterised by a different elbow-angle value, have been randomised to avoid biases. This randomization is performed for each participant.

3) Static Task: The static test is designed to evaluate muscular fatigue during isometric holds, with and without the assistance of the exosuit. Two distinct holds have been selected to introduce variation to the test: one involving flexion of the arm at $90°$, and the other abduction at $90°$. In both cases, to maximize strain, the elbow remains completely extended. The test is divided into two phases, each corresponding to one of the holds. These phases are randomized among participants to prevent biases. The experiment comprises three trials, with a 20-second rest period between each trial. During each trial, the participant is instructed to either flex or abduct the arm to $90°$ and maintain this position for 40 seconds. To speed up the onset of muscular fatigue, the test is conducted under loaded conditions, with a 1.5 kg weight band (Reebok, Bolton, United Kingdom) secured around the participant's wrist. For each phase, the subject conducted a series of three trials under two conditions: wearing the unpowered exosuit and wearing

This article has been accepted for publication in IEEE Transactions on Medical Robotics and Bionics. This is the author's version which has not been fully edited and content may change prior to final publication. Citation information: DOI 10.1109/TMRB.2025.3646763

the powered exosuit. These conditions are also randomized among participants. To avoid fatigue artefacts across conditions, a 10-minute rest period between different conditions is implemented.

B. Data Analysis

Before conducting the experiments, we gathered maximum voluntary contraction (MVC) data from the monitored muscles, to normalize the EMG signals during data analysis. The effectiveness of the device was quantified regarding its influence on muscle activity and movement kinematics. To evaluate tracking precision for each task, we computed the coefficient of determination R^2 alongside the Root Mean Square Error (RMSE) between the reference trajectories and those measured for the elbow and shoulder, recorded under two different conditions (*Exo off* and *Exo on*). The EMG signals were filtered offline with a fourth-order Bandpass Butterworth filter (cut-off frequency $15\,\text{Hz}$-$450\,\text{Hz}$), rectified and low-pass filtered at $6\,\text{Hz}$ with a fourth-order Butterworth filter; the signals were then normalized to each participant's MVC. We assessed the Root Mean Square (RMS) values, serving as an indicator of activation levels across various tasks and conditions. Moreover, to evaluate muscular fatigue, raw EMG signals were filtered between $15\,\text{Hz}$-$450\,\text{Hz}$ with a fourth-order Butterworth filter; we used the median normalized frequency (MNF) of the EMG power spectrum as an index of fatigue [29]. During the final isometric hold phase, we evaluated the metric over twenty-four $1\,\text{s}$ epochs. The time window was defined by excluding the first and last $4\,\text{s}$ of the hold phase, as these segments may contain transient-related phenomena. Additionally, another $4\,\text{s}$ were discarded at the beginning of the isometric contraction to focus on its last portion, where fatigue is more likely to manifest.

C. Statistical Analysis

We assessed the normal distribution of the measurements via a Shapiro-Wilk test with a significance level set at $\alpha = 0.05$. To evaluate statistical differences between the *Exo off* and *Exo on* conditions, repeated measures analysis of variance (rANOVA) was adopted to examine the effects on the muscles in the *Dynamic Task*. We considered the type of *'Assistance'* as within-subjects factor and the different elbow angle as the second factor. Statistical significance was considered for p-values lower than 0.05. Post-hoc analysis on significant main effects and interaction was performed using Bonferroni-corrected paired t-tests. To evaluate statistical differences between the *Exo off* and *Exo on* conditions, in the *ROM Assessment* and the *Static Task*, we used paired t-tests. Statistical significance was considered for p-values lower than 0.05. All statistical analyses were performed using Minitab (Minitab, State College, PA, USA). Reported values are presented as mean $\pm$ standard error (SE), and significant differences are marked with the symbol * in all figures.

V. Results

A. ROM assessment

Figure 5 shows the data captured by the motion capture system, both with and without the exosuit. No significant differences were observed between the exosuit and off conditions, except for pure abduction. In pure abduction, the maximum shoulder abduction with the exosuit was 84.6 ± 2.3 degrees, compared to 90.2 ± 1.4 degrees in the off condition, indicating a significant difference of 5 degrees on average. For pure flexion, the maximum shoulder flexion was 89.4 ± 1.6 degrees with the exosuit, compared to 90.4 ± 1.4 degrees without it. During the mixed condition, where the shoulder was positioned at 45 degrees between the sagittal and frontal planes, the maximum range of motion in the exosuit was 90.5 ± 0.8 degrees, compared to 89.8 ± 1.2 degrees without the exosuit. These results suggest that while the exosuit marginally affected pure abduction, it did not significantly alter shoulder mobility within the analyzed workspace.

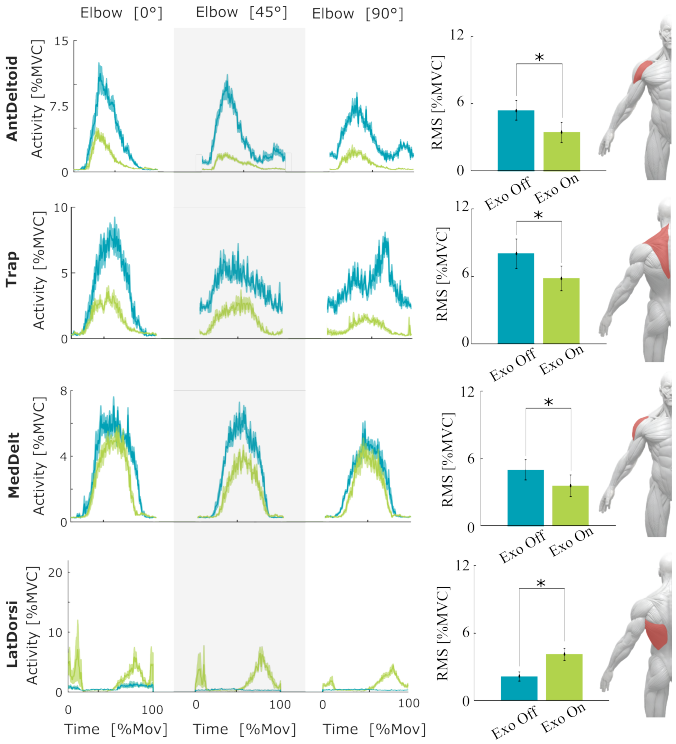

Fig. 7. *EMG* evaluation of the device during the dynamic task. From top to bottom, EMG activity of the *anterior deltoid*, *trapezius*, *medial deltoid*, and *latissimus dorsi*. On the left, temporal plot of a representative subject performing the task with the elbow positioned at $0°$, $45°$ and $90°$. On the right, Root Mean Square (RMS) of EMG activity comparing Exo Off and Exo On conditions, normalized to MVC values. Results indicate muscle activation changes across conditions, demonstrating the exosuit's impact on the main muscle groups insisting on the shoulder joint.

B. Dynamic Task

1) Kinematics: As the figure suggests, there are no significant changes in the correlation index related to the elbow flexion angle and shoulder abduction. The only significant difference ($p = 0.031$) across the two conditions (*ExoOff* and *ExoOn*, respectively 0.88 ± 0.04,$0.81 \pm 0.09 rad$) pertains to the shoulder flexion. This is confirmed by the RMSE ($p = 0.015$), where we observe an error of $0.15 \pm 0.03 rad$ in *ExoOff*, and of $0.19 \pm 0.04 rad$ in the *ExoOn* condition. The other two angles also in this case do not show significant differences with an average correlation index of 0.92 and 0.61 and RMSE

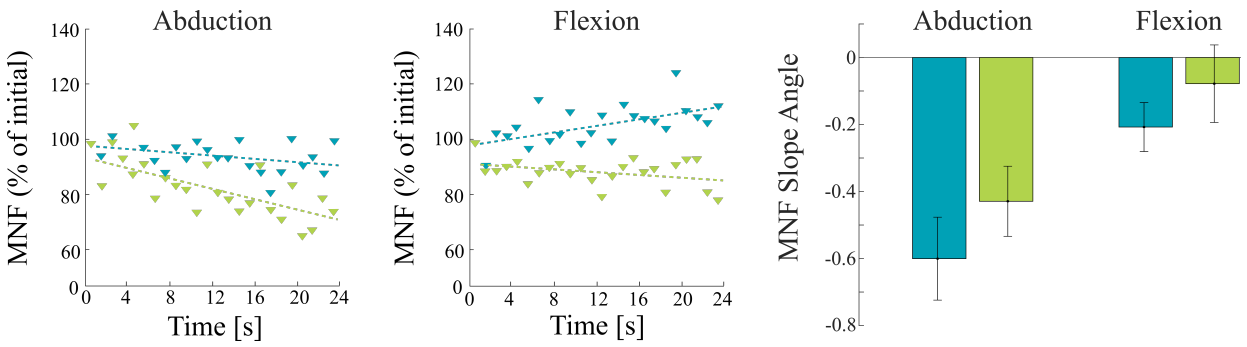

Fig. 8. *Static Task.* Effect of the exosuit on muscular fatigue across subjects. On the left side, temporal plot of the MNF of a representative subject. In the abduction phase, MNF values extracted from the medial deltoid are shown along the isometric hold phase, with fatigue evaluated over twenty-four 1 s epochs. In the flexion phase, MNF values extracted from the anterior deltoid are similarly shown along the hold phase. On the right side, the bar plot shows *Exo off* vs *Exo on* conditions for the abduction and flexion phases.

of 0.23 and 0.19 for the elbow flexion and shoulder abduction respectively. Getting assistance from the device then slightly decreases the accuracy of the movements, in particular at the shoulder flexion level, which is one of the DoFs supported by the exosuit.

2) Muscle activity: The figure suggests, that the exosuit assistance causes a significant reduction in the muscular activation of the *Anterior Deltoid, Medial Deltoid* and *Trapezius* while determining a significant increase in the activation of the *Latissimus Dorsi*. In particular, for each muscle the $mean \pm SE$ of the RMS of the activation across the two conditions (*ExoOff* and *ExoOn* is respectively: 5.41 ± 0.88, 3.45 ± 0.86 ($p = 0.023$); 5.02 ± 0.91, 3.58 ± 0.94 ($p = 0.021$); 8.00 ± 1.31, 5.82 ± 1.08 ($p = 0.020$); 2.14 ± 0.41, 4.07 ± 0.54($p = 0.018$). There were no significant changes in the *biceps* and *triceps*.

C. Static Task

The isometric contraction task, performed with assistance from the exosuit, showed a slower trend in the onset of fatigue for the anterior and medial deltoids compared to the unpowered condition, though this difference was not statistically significant. Figure 8-left displays the median frequency of the EMG spectrum (MNF) for a representative subject in the *Exo off* and *Exo on* conditions. The right side of Figure 8 shows the average slope and its standard error across subjects, separated by abduction and flexion. Specifically, the average slopes were 0.60 ± 0.12 and 0.43 ± 0.10 for the *Exo off* and *Exo on* conditions, respectively, in abduction; and 0.21 ± 0.07 and 0.08 ± 0.12 for the *Exo off* and *Exo on* conditions, respectively, in flexion.

VI. Discussion

This study demonstrates the feasibility and promise of soft tendon-driven exosuits (FALCO) in delivering lightweight, comfortable, and adaptive support for prolonged or repetitive shoulder activities, typical in occupational and everyday tasks. The findings emphasize key advantages of the exosuit design, such as its ability to reduce muscular effort and improve endurance, while also pinpointing areas that require further refinement.

FALCO combines a lightweight textile structure with tendon-driven, multi-degree-of-freedom actuation and an intuitive control system, providing a unique blend of support and mobility. This balance distinguishes it from many existing devices and makes it particularly well suited for tasks involving sustained or repetitive shoulder movements.

A key advantage of the proposed design lies in its adaptability and reconfigurable architecture, allowing it to be adjusted to accommodate various anatomical structures and movement demands. This enables tailored support for complex joints such as the hip, wrist, or ankle. Moreover, the lightweight and tendon-driven nature of the system provides a strong basis for scalability toward multi-joint or multi-degree-of-freedom configurations. The same actuation principle could be extended to support additional joints, such as the elbow or wrist, through modular tendon routing and anchor redesign, enabling coordinated upper-limb assistance. This modular expansion would preserve the system's portability and low mechanical complexity while broadening its applicability to more complex motion patterns and multi-task activities. By leveraging underactuation, the system maintains effective assistance while simplifying mechanical complexity, which reduces both weight and energy consumption. This design strategy enhances manufacturability and maintenance while also improving user-friendliness by enabling easy customization to individual needs, ultimately increasing usability and applicability across a broad range of motions.

To the best of our knowledge, this represents one of the first implementations of active reconfiguration in a tendon-driven soft exosuit that prioritizes functional alignment over direct force application. This approach improves user-system compatibility without necessitating full multi-actuator redundancy. Although a fixed-geometry baseline was not included, the consistent assistance across multi-DoF movements and maintained kinematic alignment indicate that the reconfigurable design effectively optimizes force direction and mechanical efficiency in real time. Future work will include a direct experimental or simulated comparison to quantitatively isolate the contribution of reconfigurability.

The experimental findings demonstrate that the exosuit significantly reduces activation in key shoulder muscles, specifically the anterior deltoid, medial deltoid, and trapezius, show-

ing an average reduction of 31% in muscle activity during dynamic tasks. This confirms the device's effectiveness in offloading gravitational demands on the shoulder, which is particularly beneficial for individuals performing continuous or repetitive shoulder movements. Additionally, the delayed onset of muscle fatigue during static tasks highlights FALCO's potential to provide sustained support over extended periods, making it well suited for both occupational applications and daily use.

Compared to current state-of-the-art soft exosuits, FALCO offers several notable advantages. It provides simultaneous, reconfigurable assistance across multiple degrees of freedom, with a dual-motor architecture that enables dynamic alignment of force vectors, enhancing both control precision and user comfort. In comparison to existing soft shoulder exosuits such as Harvard's pneumatic system [21] and ETH Zurich's tendon-driven design [22], which are primarily limited to single-degree-of-freedom support, FALCO uniquely combines dual-motor underactuation with reconfigurable geometry, enabling adaptive, multi-DoF gravity compensation within a lightweight structure. This configuration achieves comparable or superior reductions in muscle activity (~31%) while maintaining natural joint mobility. This approach supports multi-planar assistance using only two actuators, reducing mechanical complexity while improving adaptability. In addition, FALCO's modular mechanical design, featuring passive decoupling elements and a customizable anchor system, paired with a real-time sensing and control strategy optimized for human biomechanics, creates a flexible and reconfigurable platform that more effectively supports natural joint motion and individual variability than previous systems.

Despite these benefits, the study also reveals some challenges. The increased activation of the latissimus dorsi during assisted movements suggests a redistribution of muscular effort toward secondary muscles. This effect may stem from the unilateral assistance configuration, which could cause compensatory activation patterns on the contralateral side. Over time, such compensations might lead to muscle imbalances or discomfort, underscoring the importance of exploring bilateral assistance or more sophisticated control algorithms that promote balanced force distribution across the shoulder complex. Additionally, understanding how the exosuit influences core muscle engagement and postural control would be valuable to ensure that no unintended compensatory behaviours compromise long-term comfort or function.

Range of motion analysis indicates that the exosuit does not significantly restrict natural shoulder movement within the evaluated workspace, except for a modest decrease in maximum shoulder abduction (84.6° with the device versus 90.2° without). While this slight limitation may not impact most users, it could pose challenges for activities requiring full shoulder abduction, such as overhead reaching or certain occupational tasks. Addressing this issue through refinements in the textile interface, tendon routing, and anchoring system will be essential to preserve full range of motion while maintaining effective support. Such improvements will likely enhance the exosuit's appeal and practicality for a broader spectrum of users and use cases.

Another important observation concerns the reduced movement accuracy, particularly during shoulder roll, which points to challenges in the device's kinematic alignment with the complex multi-DoF shoulder joint. This misalignment likely arises from the interplay between the shoulder's intricate biomechanics, the compliance of the textile interface, and the Bowden cable transmission system. To address this, future design iterations should focus on improving the mechanical alignment of the exosuit with key anatomical landmarks and on developing more adaptive control algorithms that synchronise more effectively with the user's natural joint movements. Incorporating advanced sensing and real-time feedback could further enhance movement smoothness and precision. In particular, combining the existing IMU-based motion intention detection with electromyographic (EMG) inputs could enable the controller to better capture user effort and muscle activation patterns, allowing assistance to be adjusted dynamically based on physiological feedback and fatigue levels.[30] It should be noted that the damping coefficients and controller gains were determined using the Ziegler–Nichols tuning method followed by empirical fine-tuning. While this approach ensured stable and responsive behavior in the current validation, future work will explore optimization-based or adaptive tuning strategies to enhance robustness across users and different load levels.

Compared to conventional rigid exoskeletons, which are often bulky, uncomfortable, and prone to kinematic misalignment due to their fixed structures, FALCO's soft and flexible design offers superior conformity to the user's body. This compliance enhances comfort and fosters a more intuitive user experience. However, these advantages come with trade-offs: tendon-driven soft exosuits generally produce lower maximum force output and face challenges in achieving precise control. Key technical hurdles include managing nonlinear force transmission, minimizing friction losses in Bowden cables, and maintaining consistent coupling between the user and the device. Despite these challenges, FALCO's lightweight construction and low power consumption make it a strong candidate for prolonged use in both daily and occupational settings. FALCO's ability to provide gravity compensation positions it as a compelling compromise between high-torque, rigid exoskeletons and passive support systems. This balance allows users to perform shoulder-intensive tasks with reduced muscular strain, without the drawbacks of bulkier or more restrictive solutions. While the present study was conducted with healthy participants in controlled lab settings, future evaluations involving a broader user base and more realistic environments are essential to fully assess and optimize the device's performance. Continued refinement of the mechanical design and control strategies will be key to improving movement accuracy, user comfort, and muscle activation patterns, ultimately enhancing the exosuit's usability and effectiveness across a wide range of applications.

VII. Conclusions

The exosuit presented in this study demonstrates the considerable potential for reducing shoulder muscle strain and

improving endurance through intuitive gravity compensation. While the results are promising, particularly in terms of reducing muscle activation and delaying fatigue, the device's limitations in movement accuracy and secondary muscle activation point to areas for future development. With further refinement, the exosuit could become a essential tool in both occupational settings and everyday assistance for individuals with or shoulder impairments, or needing continuous support during working tasks.

ACKNOWLEDGEMENTS

This work was supported by the Deutsche Forschungsgemeinschaft through Project HIT.Reha "Human Impedance control for Tailored Rehabilitation" under Grant N505327336.

REFERENCES

[1] A. M. Halder, E. Itoi, and K.-N. An, "Anatomy and biomechanics of the shoulder," *Orthopedic Clinics*, vol. 31, no. 2, pp. 159–176, 2000.

[2] G. J. van der Heijden, "Shoulder disorders: a state-of-the-art review," *Best Practice & Research Clinical Rheumatology*, vol. 13, no. 2, pp. 287–309, 1999.

[3] R. A. Gopura and K. Kiguchi, "Mechanical designs of active upper-limb exoskeleton robots: State-of-the-art and design difficulties," in *2009 IEEE International Conference on Rehabilitation Robotics*. IEEE, 2009, pp. 178–187.

[4] H. Veeger and F. Van Der Helm, "Shoulder function: the perfect compromise between mobility and stability," *Journal of biomechanics*, vol. 40, no. 10, pp. 2119–2129, 2007.

[5] R. Gopura, D. Bandara, K. Kiguchi, and G. K. Mann, "Developments in hardware systems of active upper-limb exoskeleton robots: A review," *Robotics and Autonomous Systems*, vol. 75, pp. 203–220, 2016.

[6] D. D. Gutierrez, L. Thompson, B. Kemp, and S. J. Mulroy, "The relationship of shoulder pain intensity to quality of life, physical activity, and community participation in persons with paraplegia," *The journal of spinal cord medicine*, vol. 30, no. 3, pp. 251–255, 2007.

[7] N. Jarrassé and G. Morel, "Connecting a human limb to an exoskeleton," *IEEE Transactions on Robotics*, vol. 28, no. 3, pp. 697–709, 2011.

[8] P. Maurice, J. Čamernik, D. Gorjan, B. Schirrmeister, J. Bornmann, L. Tagliapietra, C. Latella, D. Pucci, L. Fritzsche, S. Ivaldi *et al.*, "Evaluation of paexo, a novel passive exoskeleton for overhead work," *Computer Methods in Biomechanics and Biomedical Engineering*, vol. 22, no. sup1, pp. S448–S450, 2019.

[9] I. Pacifico, A. Scano, E. Guanziroli, M. Moise, L. Morelli, A. Chiavenna, D. Romo, S. Spada, G. Colombina, F. Molteni *et al.*, "An experimental evaluation of the proto-mate: a novel ergonomic upper-limb exoskeleton to reduce workers' physical strain," *IEEE robotics & automation magazine*, vol. 27, no. 1, pp. 54–65, 2020.

[10] E. Bardi, M. Gandolla, F. Braghin, F. Resta, A. L. Pedrocchi, and E. Ambrosini, "Upper limb soft robotic wearable devices: a systematic review," *Journal of NeuroEngineering and Rehabilitation*, vol. 19, no. 1, p. 87, 2022.

[11] M. Sierotowicz, D. Brusamento, B. Schirrmeister, M. Connan, J. Bornmann, J. Gonzalez-Vargas, and C. Castellini, "Unobtrusive, natural support control of an adaptive industrial exoskeleton using force myography," *Frontiers in Robotics and AI*, vol. 9, p. 919370, 2022.

[12] L. Grazi, E. Trigili, G. Proface, F. Giovacchini, S. Crea, and N. Vitiello, "Design and experimental evaluation of a semi-passive upper-limb exoskeleton for workers with motorized tuning of assistance," *IEEE Transactions on Neural Systems and Rehabilitation Engineering*, vol. 28, no. 10, pp. 2276–2285, 2020.

[13] F. Missiroli, P. Mazzoni, N. Lotti, E. Tricomi, F. Braghin, L. Roveda, and L. Masia, "Integrating computer vision in exosuits for adaptive support and reduced muscle strain in industrial environments," *IEEE Robotics and Automation Letters*, 2023.

[14] C. Simpson, B. Huerta, S. Sketch, M. Lansberg, E. Hawkes, and A. Okamura, "Upper extremity exomuscle for shoulder abduction support," *IEEE Transactions on Medical Robotics and Bionics*, vol. 2, no. 3, pp. 474–484, 2020.

[15] C. T. O'Neill, T. Proietti, K. Nuckols, M. E. Clarke, C. J. Hohimer, A. Cloutier, D. J. Lin, and C. J. Walsh, "Inflatable soft wearable robot for reducing therapist fatigue during upper extremity rehabilitation in severe stroke," *IEEE Robotics and Automation Letters*, 2020.

[16] N. F. Rojo, I. Nazari, C. Applegate, M. Lee, J. Carley, and Y. Sun, "A wearable soft exoskeleton for shoulder motion assistance," in *2022 IEEE/ACM Conference on Connected Health: Applications, Systems and Engineering Technologies (CHASE)*. IEEE, 2022, pp. 162–163.

[17] Y. M. Zhou, C. J. Hohimer, H. T. Young, C. M. McCann, D. Pont-Esteban, U. S. Civici, Y. Jin, P. Murphy, D. Wagner, T. Cole *et al.*, "A portable inflatable soft wearable robot to assist the shoulder during industrial work," *Science Robotics*, vol. 9, no. 91, p. eadi2377, 2024.

[18] N. Lotti, F. Missiroli, E. Galofaro, E. Tricomi, D. Di Domenico, M. Semprini, M. Casadio, G. Brichetto, L. De Michieli, A. Tacchino *et al.*, "Soft robotics to enhance upper limb endurance in individuals with multiple sclerosis," *Soft Robotics*, vol. 11, no. 2, pp. 338–346, 2024.

[19] M. Xiloyannis, R. Alicea, A.-M. Georgarakis, F. L. Haufe, P. Wolf, L. Masia, and R. Riener, "Soft robotic suits: State of the art, core technologies, and open challenges," *IEEE Transactions on Robotics*, pp. 1–20, 2021.

[20] D. Park and K.-J. Cho, "Development and evaluation of a soft wearable weight support device for reducing muscle fatigue on shoulder," *PloS one*, vol. 12, no. 3, p. e0173730, 2017.

[21] T. Proietti, C. O'Neill, L. Gerez, T. Cole, S. Mendelowitz, K. Nuckols, C. Hohimer, D. Lin, S. Paganoni, and C. Walsh, "Restoring arm function with a soft robotic wearable for individuals with amyotrophic lateral sclerosis," *Science Translational Medicine*, vol. 15, no. 681, p. eadd1504, 2023.

[22] A.-M. Georgarakis, M. Xiloyannis, P. Wolf, and R. Riener, "A textile exomuscle that assists the shoulder during functional movements for everyday life," *Nature Machine Intelligence*, vol. 4, no. 6, pp. 574–582, 2022.

[23] F. Missiroli, N. Lotti, E. Tricomi, C. Bokranz, R. Alicea, M. Xiloyannis, J. Krzywinski, S. Crea, N. Vitiello, and L. Masia, "Rigid, soft, passive, and active: A hybrid occupational exoskeleton for bimanual multijoint assistance," *IEEE Robotics and Automation Letters*, vol. 7, no. 2, pp. 2557–2564, 2022.

[24] K. M. Lynch and F. C. Park, *Modern robotics*. Cambridge University Press, 2017.

[25] M. Katayama and M. Kawato, "Virtual trajectory and stiffness ellipse during multijoint arm movement predicted by neural inverse models," *Biological cybernetics*, vol. 69, no. 5-6, pp. 353–362, 1993.

[26] A. Q. Keemink, H. Van der Kooij, and A. H. Stienen, "Admittance control for physical human–robot interaction," *The International Journal of Robotics Research*, vol. 37, no. 11, pp. 1421–1444, 2018.

[27] K. R. Holzbaur, W. M. Murray, and S. L. Delp, "A model of the upper extremity for simulating musculoskeletal surgery and analyzing neuromuscular control," *Annals of biomedical engineering*, vol. 33, pp. 829–840, 2005.

[28] R. M. Chapman, M. T. Torchia, J.-E. Bell, and D. W. Van Citters, "Assessing shoulder biomechanics of healthy elderly individuals during activities of daily living using inertial measurement units: high maximum elevation is achievable but rarely used," *Journal of biomechanical engineering*, vol. 141, no. 4, p. 041001, 2019.

[29] R. Merletti and P. Parker, *Electromyography : physiology, engineering, and noninvasive applications*, 11th ed. Wiley-IEEE Press, 2004.

[30] W. Wang, H. Ren, S. Su, P. Zhang, and J. Zhang, "A brain-inspired decision-making method for upper limb exoskeleton based on multi-brain-region structure and multimodal information fusion," *Measurement*, vol. 241, p. 115728, 2025.